Performance of DG methods based on different variables for low Mach number flows

Nicolas Chauchat, Roland Becker, Éric Schall

Commun Nonlinear Sci Numer Simulat xxx (xxxx) xxx

Contents lists available at ScienceDirect

Commun Nonlinear Sci Numer Simulat

journal homepage: www.elsevier.com/locate/cnsns

Research paper

Performance of DG methods based on different variables for low Mach number flows

Nicolas Chauchat[a,*], Roland Becker[b], Eric Schall[a]

[a] Universite de Pau et des Pays de l'Adour, E2S UPPA, SIAME, Pau, France
[b] Universite de Pau et des Pays de l'Adour, E2S UPPA, CNRS, LMAP, Pau, France

ARTICLE INFO

Article history:
Received 10 March 2020
Revised 16 September 2020
Accepted 19 October 2020
Available online xxx

Keywords:
Discontinuous Galerkin finite elements method (DGFEM)
Euler equations
Entropy variables
Primitive variables
Incompressible limit
Low Mach number

ABSTRACT

Based on its good theoretical properties, the use of entropy variables is an excellent choice for computing compressible flows at low Mach number. In this paper, we discuss the use of entropy variables in a discontinuous Galerkin discretization of the compressible Euler equations and generalize the numerical flux proposed by Barth to physical and conservative variables. Next, we compare the DG0 discretization based on the entropy variables with several other DG0 discretizations, and also with a standard finite volume method. Comparisons of DG1 discretization with the different sets of variables give hope in an all-Mach number solver.

1. Introduction

The discretization of the Euler equations [1] is generally based on conservative variables, since they allow the equations to be written as a hyperbolic system. However, several formulations have been proposed for various reasons.

In the context of finite element methods, Barth [2] used entropy variables [3] in order to construct an entropy-stable discretization. The reason for this was that the discrete equations can be tested with these variables, whereas the nonlinearity of the change of variables leads to additional interpolation errors, unless the approximation is piecewise constant, which is the case for cell-centered finite volumes and discontinuous Galerkin (DG) at the lowest order.

It is also well known that the system written in conservative variables degenerates in the incompressible limit and the change of variables becomes singular, see Hauke and Hughes [4] and Pesch and van der Vegt [5]. In view of this difficulty, the latter articles developed stable methods for continuous and discontinuous finite element approximations, both based on a combination of entropy variables and physical variables. We should, however, mention that the discretization of the diffusion in the compressible Navier-Stokes equations is considerably easier in physical variables than in entropy variables.

The purpose of this article is to present numerical experiments illustrating different aspects of the choice of variables in the context of the discontinuous Galerkin method. Our method is based on the entropy-stable flux [6] of in combination with the change of variables developed in Pesch and van der Vegt [5]. This leads to identical discrete solutions in the lowest-order case DG0 and allows for fair comparisons for higher-order discretizations DG1. Since this numerical flux is different from standard approaches, our first concern is the comparison of the proposed method with the HLLC flux [7] and

* Corresponding author.
E-mail addresses: nicolas.chauchat@univ-pau.fr (N. Chauchat), roland.becker@univ-pau.fr (R. Becker), eric.schall@univ-pau.fr (E. Schall).

https://doi.org/10.1016/j.cnsns.2020.105580
1007-5704/

the Roe-based [8] finite volume solver in FLUENT [9]. Our second topic is the comparison of the different sets of variables: conservative, entropy, and physical variables. Although the discrete solutions coincide in the lower case (i.e. DG0), the non-linearities are different and have an influence on the practical behavior of the methods.

Finally, our third topic is the behavior of the different methods at low Mach numbers [10,11]. Since the theory of numerical methods for the Euler equations in the incompressible limit [12] is not complete, computational experiments are important.

The article is organized as follows. We close this section with some notation. Sections 2 and 3 describe the proposed DG discretization with different sets of variables. The Jacobians required for the numerical fluxes are given in Appendix. Section 4 presents comparisons between the proposed numerical flux and standard approaches based on the Roe-FVM and HLLC-DGFEM discretizations. For a fair comparison, we use the lowest order DG approximation DG0, which is very close to cell-centered finite volumes. Then in Section 5 we compare the use of different variables in the DG method using well-known test problems for low Mach number flows. We also consider the higher-order approximations DG1, but restrict ourselves to cases without shocks, in order to focus on the role of the choice of variables. Higher-order DG discretizations for shock problems would require additional slope-limiters [13], obscuring the comparison.

Finally, we draw some conclusions on the numerical experiments presented in this article in Section 6.

1.1. Notation

We denote by $v \cdot w$ the Euclidian scalar product for $v, w \in \mathbb{R}^n$ (which are column vectors), and by $|\cdot|$ the associated norm. We frequently use the notation $v^{\mathsf{T}} w = v \cdot w$. We denote the transpose of a matrix $A \in \mathbb{R}^{n\times m}$ by A^{T}.

For a differentiable function $f : A \subset \mathbb{R}^n \to \mathbb{R}^m$ we denote by Df its Jacobian matrix, $(Df)_{ij} = \frac{\partial f_i}{\partial u_j}$. In the special case $m = 1$ we let $\nabla f = Df^{\mathsf{T}}$. In particular, we have for $g(u) = f(T(u))$ that $\nabla g = (DfDT)^{\mathsf{T}} = DT^{\mathsf{T}} \nabla f$.

Let $\phi : \mathbb{R}^n \to \mathbb{R}$, $f : \mathbb{R}^n \to \mathbb{R}^n$ and $\phi(u) := u \cdot f(u)$. Then $D\phi = f(u) + u^{\mathsf{T}} Df$, since

$$\frac{\partial \phi}{\partial u_i} = \sum_{k=1}^{n} \frac{\partial (u_k f_k(u))}{\partial u_i} = \sum_{k=1}^{n} \left(\delta_{ik} f_k(u) + u_k \frac{\partial f_k(u)}{\partial u_i} \right) = f_i(u) + \left(u^T Df \right)_i.$$

2. The Euler equations as a hyperbolic system

We consider the classical Euler equations for an ideal gas $p/\rho = RT$ [14]. Let ρ, V, p, T and E be the density, velocity, pressure, temperature and total energy respectively. The Euler equations expressed as a system of mass and momentum and energy conservation equations read:

$$\begin{aligned} &\frac{\partial \rho}{\partial t} + \operatorname{div}(\rho V) = 0, \\ &\frac{\partial \rho V}{\partial t} + \operatorname{div}(\rho V \otimes V) + \nabla p = 0, \\ &\frac{\partial \rho E}{\partial t} + \operatorname{div}(\rho V E) + \operatorname{div}(pV) = 0. \end{aligned} \tag{1}$$

We write (1) as a system of hyperbolic equations in the conservative variables

$$u = \begin{pmatrix} \rho \\ \rho V \\ \rho E \end{pmatrix} \tag{2}$$

with the help of smooth flux functions $f_i : A \to \mathbb{R}^m$, $(A \subseteq \mathbb{R}^m)$ $1 \le i \le d$

$$\frac{\partial u}{\partial t} + \sum_{i=1}^{d} \frac{\partial f_i(u)}{\partial x_i} = 0 \tag{3}$$

combined with the initial condition

$$u(0) = u_0 \tag{4}$$

and appropriate boundary conditions. The quasi-linear form of (3) uses the flux Jacobians $A_i(u) = Df_i(u)$:

$$\frac{\partial u}{\partial t} + \sum_{i=1}^{d} A_i(u) \frac{\partial u}{\partial x_i} = 0 \tag{5}$$

Eq. (3) is understood in the weak sense, since the solutions are in general not differentiable and even discontinuous (formation of shocks). From a mathematical point of view, a weak formulation is therefore considered, where all the derivatives are put on smooth test functions via integration by parts.

For the Cauchy problem ($\Omega = \mathbb{R}^n$), this reads for example: Find $u \in L^1([0;+\infty[\times\mathbb{R}^n)$ such that for all smooth compactly supported test functions ϕ

$$\int_0^\infty \int_{\mathbb{R}^n} \left(u\frac{\partial \phi}{\partial t} + \sum_{i=1}^{d} f_i(u) \cdot \frac{\partial \phi}{\partial x_i} \right) = \int_{\mathbb{R}^n} u_0 \phi(0)$$

The mathematical theory of hyperbolic systems in several space dimensions is still incomplete. The situation is much more satisfactory for scalar equations. In order to obtain uniqueness of the weak solution, they must satisfy an additional entropy condition.

If u is a piecewise smooth solution with a surface of discontinuity Γ, the weak formulation implies the Rankine-Hugoniot condition, which determines the shock speed s :

$$s[u] = [f_n(u)] \tag{6}$$

where [.] is the jump.

The system is hyperbolic if the Jacobian $A_n = Df_n(u) = \sum_{i=1}^{d} A_i'(u) n_i$ admits a spectral decomposition

$$A_n(u) = R_n(u)\Lambda_n(u)R_n(u)^{-1} \tag{7}$$

with a real diagonal matrix of eigenvalues $\Lambda(u)$ and a regular matrix $R_n(u)$ composed of the eigenvectors of A_n for all vectors $n \in \mathbb{R}^d$.

Since hyperbolicity is conserved under a smooth change of variables $u = \Phi(w)$, the quasilinear system can be transformed into

$$D\Phi(w)\frac{\partial w}{\partial t} + \sum_{i=1}^{d} A_i(u(w))D\Phi(w)\frac{\partial w}{\partial x_i} = 0. \tag{8}$$

It is called symmetric if $D\Phi(w)$ is symmetric positive definite and matrices $A_i(u(w))D\Phi(w) = g_i'(w)$, $g_i(w) := f_i(u(w))$ are symmetric.

The system admits a mathematical entropy if there is a pair of smooth functions (U, F) $U : A \to \mathbb{R}$, $F_i : A \to \mathbb{R}$ $(1 \le i \le d$, $A \subset \mathbb{R}^m)$ such that U is strictly convex and for all i

$$DU(u)Df_i(u) = DF_i(u). \tag{9}$$

The existence of an entropy for the Euler equations is crucial and follows from thermodynamics. It implies hyperbolicity and the possibility to symmetrize the system.

We impose that the entropy is a decreasing function of time (the physical entropy, which is more or less its negative, is increasing):

$$\frac{\partial U(u)}{\partial t} + \sum_{i=1}^{d} \frac{\partial F_i(u)}{\partial x_i} \le 0 \tag{10}$$

Since solutions develop shocks, (10) has again to be understood in a weak sense. Similarly as before we get the Rankine-Hugoniot condition [15] for entropy:

$$s[U(u)] \le [F_n(u)] \tag{11}$$

For a smooth solution we do have an equality in (10) thanks to (9):

$$\begin{aligned}
\frac{\partial U(u)}{\partial t} + \sum_{i=1}^{d} \frac{\partial F_i(u)}{\partial x_i} &= DU(u)\frac{\partial u}{\partial t} + \sum_{i=1}^{d} DF_i(u)\frac{\partial u}{\partial x_i} \\
&= DU(u)^{\mathsf{T}} \cdot \frac{\partial u}{\partial t} + \sum_{i=1}^{d} DU(u)Df_i(u)\frac{\partial u}{\partial x_i} \\
&= DU(u)^{\mathsf{T}} \cdot \left(\frac{\partial u}{\partial t} + \sum_{i=1}^{d} \frac{\partial f_i(u)}{\partial x_i} \right) = 0.
\end{aligned}$$

2.1. Entropy variables

The Legendre-Fenchel transform [16] of $U(u)$, $U^*(v)$, is defined by $U^*(v) = \sup_u (u \cdot v - U(u)) = u(v) \cdot v - U(u(v))$ with $DU(u(v)) = v^{\mathsf{T}}$ and is called entropy potential. Then we have

$$DU^*(v) = u(v)^{\mathsf{T}} + v^{\mathsf{T}}\frac{\partial u}{\partial v} - DU\frac{\partial u}{\partial v} = u(v)^{\mathsf{T}}. \tag{12}$$

Since the conjugate of a smooth convex function is a smooth convex function, it follows that $M := M(v) = \frac{\partial u}{\partial v} = D^2U^*(v)$ is symmetric positive-definite and A_n is similar to

$$M^{-1/2}A_nM^{1/2} = M^{-1/2}(A_nM)M^{-1/2}. \tag{13}$$

which is symmetric, since A_nM is symmetric as we will see below, and the hyperbolicity of the system follows.

The mapping $v \to u(v)$ is a special change of variables and we call $v = DU^\mathsf{T}$ the entropy variables in contrast to the conservative variables u. Clearly $V(u) = U(u(v))$ is convex since $D^2V = I$. Let $g_i(v) := f_i(u(v))$, and $G_i(v) := F_i(u(v))$. Then

$$DG_i(v) = DF_i(u(v))M(v) = DU(u(v))Df_i(u(v))M(v) = DU(v)Dg_i(v). \tag{14}$$

This change of variables transforms the quasilinear form (5) into

$$M(v)\frac{\partial v}{\partial t} + \sum_{i=1}^{d} C_i(v)\frac{\partial v}{\partial x_i} = 0 \quad \text{at } \Omega, \tag{15}$$

with $M(v)$ symmetric positive definite and $C_i(v) := Dg_i(v) = Df_i(u(v))M(v)$ symmetric, as will be seen below. Therefore, the entropy variables symmetrize the system. The equivalence between the existence of a generalized entropy and symmetrizability of the equations has been shown in Mock [17] and Godunov [18,19].

The symmetry of the Jacobian in entropy variables remains to be seen. The entropy potential $F_i^*(v)$ is defined such that

$$F_i(u) + F_i^*(v) = f_i(u)\cdot v \quad \text{resp.} \quad G_i(v) + F_i^*(v) = g_i(v)\cdot v \tag{16}$$

It follows from Eq. (14) that

$$DF_i^*(v) = g_i(v)^\mathsf{T} + v^\mathsf{T}C_i(v) - DG_i(v) = g_i(v)^\mathsf{T} \tag{17}$$

From this identity follows the symmetry of $C_i(v) = Dg_i(v) = D^2F_i^*(v)$.

In addition to symmetrizing the system, the use of entropy variables avoids problems of Jacobian definition when the Mach number tends to 0. Indeed, Hauke and Hugues [4] showed that the Jacobian limit is not defined in conservative variables when the Mach number tends to 0. For example, in 1D:

$$\lim_{M\searrow 0} A_1(u) = \begin{pmatrix} 0 & 1 & 0 \\ +\infty & \mp\frac{0}{0} & \pm\frac{0}{0} \\ \pm\infty & -\frac{0}{0} & \pm\frac{0}{0} \end{pmatrix}, \tag{18}$$

while we do not encounter this problem in entropy variables.

In the following, the entropy vector will correspond to the following vector:

$$v = \begin{pmatrix} \dfrac{\tilde{\mu} - \frac{1}{2}|V|^2}{T} \\ \dfrac{V}{T} \\ \dfrac{-1}{T} \end{pmatrix}, \tag{19}$$

with $\tilde{\mu} = h - Ts$ the chemical potential of the fluid, V the velocity, T the temperature, h the enthalpy and s the entropy. For a perfect gas, the entropy variables can be written as:

$$v = \begin{pmatrix} \dfrac{c_pT(1-\ln(T)) + RT(\ln(p) - \ln(R)) - \frac{1}{2}|V|^2}{T} \\ \dfrac{V}{T} \\ \dfrac{-1}{T} \end{pmatrix} \tag{20}$$

with p the pressure, c_P the specific heat at constant pressure and R the perfect gas constant.

2.2. Primitive variables

Next to the entropy variables, the primitive variables [20] also have a well-defined Jacobian when the Mach number tends to 0, but the primitive variables do not symmetrize the system. The primitive variables are defined as:

$$y = \begin{pmatrix} p \\ V \\ T \end{pmatrix}. \tag{21}$$

3. Approximation with discontinuous finite elements

In this section the written formalism is the one that the mathematical community used. Symbols and operators are described in the appendix.

Let $\mathcal{H}$ be a family of admissible regular meshes in the usual sense. A mesh h consists of cells $\mathcal{K}_h$. We denote by $\mathcal{S}_h^{\text{int}}$ the set of interior faces and we put $\mathcal{S}_h = \mathcal{S}_h^{\text{int}} \cup \mathcal{S}_h^{\partial}$. The measure of K (or $S \in \mathcal{S}_h$) is denoted by $|K|$ ($|S|$ respectively).

For an interior face S, n_S is a fixed unit vector normal to S. If the face S lies on $\partial\Omega$, we set $n_S = n_\Omega$, the outward pointing unit normal vector.

We define the spaces of piecewise polynomial functions of degree $k \in \mathbb{N}$ on elements:

$$D_h^k := \left\{ v_h \in L^2(\Omega) : \ v_h|_K \in P^k(K) \ \forall K \in \mathcal{K}_h \right\}.$$

Let $u \in D_h^k$. We define for a given interior face $S \in \mathcal{S}_h^{\text{int}}$ and $x \in S$

$$u_S^{\text{in}}(x) := \lim_{\varepsilon \searrow 0} u(x - \varepsilon n_S), \quad u_S^{\text{ex}}(x) = \lim_{\varepsilon \searrow 0} u(x + \varepsilon n_S).$$

Next, we define the jump and mean for $x \in S$ by

$$[u](x) := u_S^{\text{in}}(x) - u_S^{\text{ex}}(x),$$

$$\{u\}(x) := \frac{1}{2}\left(u_S^{\text{in}}(x) + u_S^{\text{ex}}(x)\right),$$

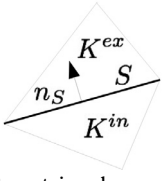

such that n_S is oriented from K^{in} towards K^{ex}, the two triangles containing the side S.

For the sake of brevity, we use the following notation for piecewise integration:

$$\int_{\mathcal{K}_h} = \sum_{K \in \mathcal{K}_h} \int_K \quad \text{and} \quad \int_{\mathcal{S}_h} = \sum_{S \in \mathcal{S}_h} \int_S.$$

We will first consider discretization of the Euler equations in conservative variables based on the approximation space $(D_h^k)^m$, i.e., we are looking for a piecewise polynomial discontinuous vector of unknowns u_h, the components of which are approximations to ρ, ρV and ρE. Note that in the lowest-order case $k = 0$ this yields approximations ρ_h, V_h, E_h (and p_h) to the physical quantities. For $k > 0$ we generally do not have polynomial approximations to v_h and E_h.

First, we define a form $a_h : (D_h^k)^m \times (D_h^k)^m \to \mathbb{R}$ by

$$a_h(u_h)(\phi_h) := -\int_{\mathcal{K}_h} \sum_{i=1}^{d} f_i(u_h) \cdot \frac{\partial \phi_h}{\partial x_i} + \int_{\mathcal{S}_h^{\text{int}}} f_{n_S}^{\Sigma}(u_h^{\text{in}}, u_h^{\text{ex}}) \cdot [\phi_h] + \int_{\mathcal{S}_h^{\partial}} f_{n_S}^{\partial}(u_h^{\text{in}}, u^{\text{D}}) \phi_h, \tag{22}$$

with an interior flux f_n^{Σ} and a boundary flux f_n^{∂}. Since the sign of the jump term (and the definition of $\cdot^{\text{in}}$ and $\cdot^{\text{ex}}$) depends on the orientation of n_S, we require

$$f_{-n}^{\Sigma}(u_h^{\text{ex}}, u_h^{\text{in}}) = f_n^{\Sigma}(u_h^{\text{in}}, u_h^{\text{ex}}), \tag{23}$$

in order for a_h to be independent of the choice of the normal.

In addition, the internal flux is supposed to verify the consistency condition

$$f_{n_S}^{\Sigma}(u, u) = f_n(u). \tag{24}$$

We now consider the semi-discrete problem

$$\left\langle \frac{\partial u_h}{\partial t}, \phi_h \right\rangle + a_h(u_h)(\phi_h) = 0 \quad \forall \phi_h \in D_h^k. \tag{25}$$

Complete discretization is achieved if we use an approximation of the time derivative by one of the classical methods. In general, we will use the implicit Euler method which amounts to

$$\left\langle \frac{u_h^n - u_h^{n-1}}{\Delta t}, \phi_h \right\rangle + a_h(u_h^n)(\phi_h) = 0 \quad \forall \phi_h \in D_h^k, \tag{26}$$

for the time steps $n = 1, 2, \ldots$ and an approximation u_h^0 of the initial data.

The definition of the internal fluxes is crucial for the entropy-stability of the method (E-flux, see Tadmor [21]).

We consider upwind fluxes of the form

$$f_n^{\Sigma}(u^{\text{in}}, u^{\text{ex}}) = \{f_n(u)\} + D^{\Sigma}(u^{\text{in}}, u^{\text{ex}})[u], \tag{27}$$

which trivially fulfill the conditions (23) and (24). The dissipation matrix D^{Σ} can be defined in many ways; the simplest choice is the diagonal matrix scaled by the maximum absolute eigenvalues (Lax-Friedrich). Another classical example is

Table 1
Physical quantities in the Euler equations, their symbol, magnitude and formula in terms of the recurrent set $\{\rho_\infty, a_\infty, T_\infty, L\}$.

Quantity	Symbol	Magnitude	Formula
mass	m	$[M]$	$\rho_\infty L^3$
length	x	$[L]$	L
time	t	$[T]$	L/a_∞
absolute temperature[1]	T	$[\theta]$	T_∞
density	ρ	$[ML^{-3}]$	ρ_∞
velocity	V	$[LT^{-1}]$	a_∞
total internal energy	E	$[L^2T^2]$	$(a_\infty)^2$
pressure	p	$[ML^{-1}T^{-2}]$	$\rho_\infty(a_\infty)^2$
specific heats	c_v, c_p	$[L^2T^{-2}\theta^{-1}]$	$(a_\infty)^2/T_\infty$

[1] Do not confuse the symbol T for temperature with the magnitude time $[T]$.

given by the Roe flux [8]. In the lowest-order case $k = 0$, the DG method is closely related to cell-centered finite volumes, and any of the fluxes developed in this context, such as approximate Riemann solvers (HLLC), can also be used.

In our implementation, we use an integral of the absolute value matrix function, see below.

For the boundary fluxes, we follow a similar approach with one of the states defined by the boundary conditions.

3.1. Change of variables

Next we consider the discretization for a change of variables. Let w be another set of variables, either the entropy variables $v = DU(u)^\mathsf{T}$ or the primitive variables $y = (p, V, T)$. In order to simplify notation, the change of variables to the conservative variables is simply written as $u(w)$.

The semi-discretization looks for $w_h \in D_h^k$ such that

$$\left\langle \frac{\partial u(w_h)}{\partial t}, \phi_h \right\rangle + a_h(w_h)(\phi_h) = 0 \quad \forall \phi_h \in D_h^k, \tag{28}$$

with

$$a_h(w_h)(\phi_h) := -\int_{\mathcal{K}_h} \sum_{i=1}^{d} f_i(u(w_h)) \cdot \frac{\partial \phi_h}{\partial x_i} + \int_{\mathcal{S}_h^{\text{int}}} f_{n_s}^{\Sigma}(w_h^{\text{in}}, w_h^{\text{ex}}) \cdot [\phi_h] + \int_{\mathcal{S}_h^{\partial}} f_{n_s}^{\partial}(w_h^{\text{in}}, w^{\text{D}})\phi_h \tag{29}$$

The first observation is that the contribution involving the time derivative is nonlinear:

$$\left\langle \frac{\partial u(w_h)}{\partial t}, \phi_h \right\rangle = \left\langle \frac{\partial u(w_h)}{\partial w} \frac{\partial w_h}{\partial t}, \phi_h \right\rangle. \tag{30}$$

In the following simulations, an implicit Euler method is used and the solution for each time step will be calculated using a Newton method. The linear system used in the Newton method is expressed in the dimensionless form as will be explained in Section 3.2.

The second observation concerns the internal flux function

$$f_n^{\Sigma}(w^{\text{in}}, w^{\text{ex}}) = \{f_n(u(w))\} + D^{\Sigma}(w^{\text{in}}, w^{\text{ex}})[w], \tag{31}$$

Different choices are possible for the dissipation matrix D^{Σ}. The choices made in this work are presented in Section 3.3

3.2. Non-dimensionalization of the Euler equation

The magnitudes of the physical quantities involved in the Euler equations can be expressed in terms of the four fundamental magnitudes: mass $[M]$, length $[L]$, time $[T]$ and temperature $[\theta]$. According to Buckingham's Pi theorem [22], the dimensionless form of the equations is obtained using a recurrent set of four reference values; we choose the set $\{\rho_\infty, a_\infty, T_\infty, L\}$, where a_∞ is the free-stream speed of sound defined as:

$$a_\infty = \sqrt{\frac{\gamma\, p_\infty}{\rho_\infty}} \tag{32}$$

and L is the characteristic length scale of the problem.

Table 1 gives the relation between the dimensional and dimensionless quantities (denoted with a tilde), for example $p = \rho_\infty (a_\infty)^2 \tilde{p}$.

Using these formulas, the dimensionless equations can be obtained by replacing the dimensional quantities by their expression in terms of the reference values and the dimensionless quantities. Eq. (33) is the dimensionless equations for the 1D Euler equation with the conservative variables.

$$\begin{pmatrix} \frac{\rho_\infty a_\infty}{L} & 0 & 0 \\ 0 & \frac{\rho_\infty (a_\infty)^2}{L} & 0 \\ 0 & 0 & \frac{\rho_\infty (a_\infty)^3}{L} \end{pmatrix} \left(\frac{\partial}{\partial \tilde{t}} \begin{pmatrix} \tilde{\rho} \\ \tilde{\rho}\tilde{V} \\ \tilde{\rho}\tilde{E} \end{pmatrix} + \frac{\partial}{\partial \tilde{x}} \begin{pmatrix} \tilde{\rho}\tilde{V} \\ (\tilde{\rho}\tilde{V}^2 + \tilde{p}) \\ \tilde{V}(\tilde{\rho}\tilde{E} + \tilde{p}) \end{pmatrix} \right) = 0 \tag{33}$$

For inviscid aerodynamics applications, the following six parameters define the flow problem [23]:

- the characteristic length scale L,
- the free-stream density ρ_∞, velocity V_∞ and temperature T_∞,
- the gas constant R and the specific heat at constant pressure c_p.

Since the equations contain four fundamental magnitudes, two dimensionless Pi groups can be formed according to Buckingham's Pi theorem. There are:

- the free-stream Mach number $M_\infty = V_\infty / a_\infty$,
- the ratio of specific heats $\gamma = c_p / c_v$,

with the set of four reference values, these are the inputs for our computations. The values of the other parameters required in the simulation are calculated using:

$$V_\infty = M_\infty a_\infty \tag{34}$$

$$p_\infty = \frac{\rho_\infty (a_\infty)^2}{\gamma} \tag{35}$$

$$R = \frac{p_\infty}{\rho_\infty T_\infty} \tag{36}$$

$$c_p = \frac{\gamma}{\gamma - 1} R \tag{37}$$

3.3. Numerical flux

In order to obtain entropy-stability, we wish to choose (for general variables) the test function $\phi_h = v(w_h)$. This form is particularly interesting for the choice of entropy variables, since $\phi_h \in D_h^k$. For other variables this is only possible for $k = 0$. Next, choosing $w = v$, we immediately obtain the numerical dissipation for the entropy, and a theoretical sound choice, see Barth [24,25], is

$$D^\Sigma(v^{\text{in}}, v^{\text{ex}}) = \int_0^1 R_n(v_s) |\Lambda_n(v_s)| R_n(v_s)^\top \, ds, \tag{38}$$

where $v_s := (1-s)v^{\text{in}} + s v^{\text{ex}}$. In practice, the integral is approximated by numerical integration.

In the case of primitive variables (and also conservative variables), we obtain an entropy flux using the transformation to entropy variables

$$D^\Sigma(w^{\text{in}}, w^{\text{ex}}) = D^\Sigma(v^{\text{in}}, v^{\text{ex}}) \int_0^1 \frac{\partial v(w_s)}{\partial w} \, ds. \tag{39}$$

The numerical integration is performed with the Simpson method which uses three integration points to calculate (38) and with a two-point integration method to calculate $\int_0^1 \frac{\partial v(w_s)}{\partial w} \, ds$.

If we compute the flow around a circular cylinder at the Mach number 3 on a quadrilateral mesh with 1680 elements and $k = 0$ and do not use sufficiently accurate quadrature rules, as indicated in the previous paragraph then an unphysical Carbuncle solution is obtained.

With entropy variables and the Simpson method for each integral, the solution obtained in Fig. 1 shows the presence of this phenomenon. On the other hand, using the proposed integration method, the solution in Fig. 2 does not have any Carbuncle.

4. Comparison of finite elements method DG0 and finite volume method (FLUENT)

In order to compare the discontinuous Galerkin finite elements method and the numerical flux presented in Section 3.3 with the existing method, two stationary test cases are considered: external Naca0012 airflow and Internal low speed nozzle. These two test cases are fundamentally different. This is a real challenge for the presented method to achieved accurate solutions whatever the flow pattern. For a fair comparison, we use the lowest-order DG approximation

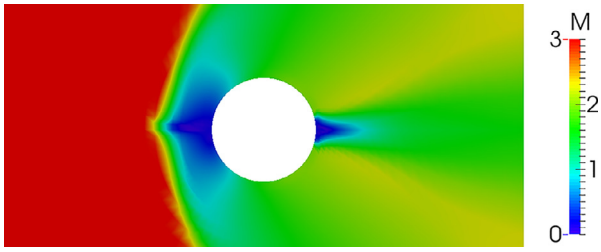

Fig. 1. Flow around a circular cylinder at Mach number 3 with DG0 and entropy variables and Simpson method for each integral of the numerical flux.

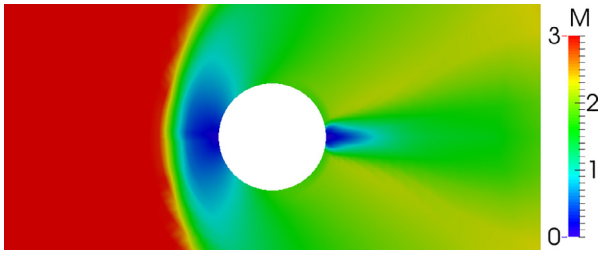

Fig. 2. Flow around a circular cylinder at Mach number 3 with DG0 and entropy variables and the proposed integration method for the numerical flux.

Table 2
Summary of test cases.

Test case	Mach number	Compressibility	State	Analytical solution
Naca0012 airflow	10^{-3} and 10^{-1}	Incompressible	Steady	No
Internal low speed nozzle	0.0036 and 0.036	Incompressible	Steady	Yes

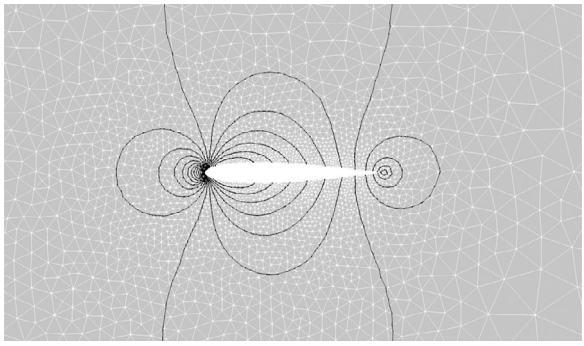

Fig. 3. Pressure field NACA0012 airfoil at Mach 10^{-1}, Fluent, $p_{\min} = 71.2294$ Pa, $p_{\max} = 71.7836$ Pa.

(i.e. DG0), which is very close to cell-centered finite volumes. These test cases consider 2D inviscid flows without thermal diffusion. Because of the low Mach number considered in these test cases, which ranges from 10^{-3} to 10^{-1}, the flow can be considered nearly incompressible. It is worth noting that the set of equations used to make the computations is that of the compressible model. This demonstrates the robustness and the accuracy of the presented method at low mach number. A description of the test cases can be found in Table 2.

These test cases allow a comparison between the finite volume method with a Roe flux (without any low Mach number preconditioner) and two discontinuous Galerkin finite element formulations, one with the HLLC flux and the other with the new flux presented in Section 3.3. The finite volume method with a Roe flux used here is implemented in the ANSYS-Fluent code.

4.1. Naca0012 airflow

In [10], Guillard and Viozat studied the flow around a NACA0012 airflow at several low Mach numbers. They showed by a first-order accurate finite volume method that with a Roe approximate Riemann flux, the pressure field shows fluctuation at low Mach numbers. They proposed a preconditioned dissipation matrix to obtain acceptable results.

Here, we study the same test case with a finite volume method and discontinuous Galerkin finite elements method.

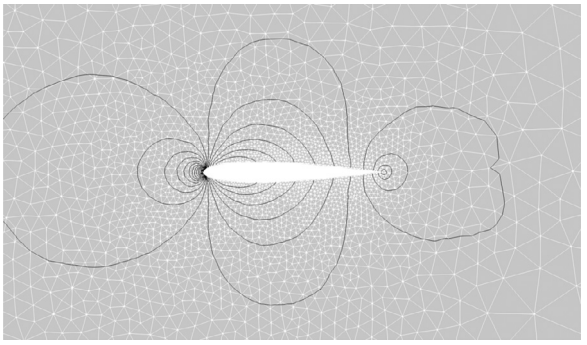

Fig. 4. Pressure field NACA0012 airfoil at Mach 10^{-1}, DG0 HLLC, $p_{\min} = 71.2312$ Pa, $p_{\max} = 71.8171$ Pa.

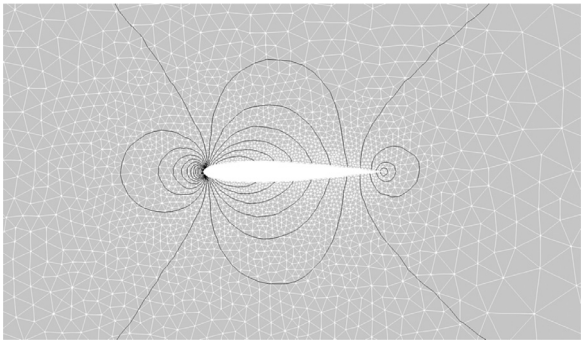

Fig. 5. Pressure field NACA0012 airfoil at Mach 10^{-1}, DG0 CONS, $p_{\min} = 71.4286$ Pa, $p_{\max} = 71.5148$ Pa.

Table 3
Pressure extrema for each simulation.

		$p_{\min}$	$p_{\max}$
Mach	Fluent	71.2294 Pa	71.7836 Pa
10^{-1}	DG0 HLLC	71.2312 Pa	71.8171 Pa
	DG0 CONS	71.4286 Pa	71.5148 Pa
Mach	Fluent	714285 Pa	714286 Pa
10^{-3}	DG0 HLLC	714285 Pa	714286 Pa
	DG0 CONS	714285 Pa	714286 Pa

All computations are done on a mesh with 7124 triangles. The dimensionless inflow velocity and density are set equal to one. The inflow pressure is chosen such that the Mach number is 10^{-1} and 10^{-3}, respectively. A comparison of the different solutions is shown for the contour of the normalized pressure $p_{norm} = (p - p_{\min})/(p_{\max} - p_{\min})$. The pressure extrema for each simulation are shown in Table 3.

Figs. 6 and 10 show the residuals for each calculation. In each case we converge as much as possible in order to reduce the residual to values below 10^{-12}. For both numerical fluxes, the discontinuous Galerkin method converges for the Mach number 10^{-1} and the simulations converge in 50 iterations. The finite volume method, however, converges only after 5000 iterations. For the Mach number 10^{-3}, convergence is better with the entropy variables-based flux than with the HLLC flux. The finite volume method requires 10 times more iterations to reach a converged solution.

High order DG implicit methods are well know to be efficient in computing iteration [26].

The solutions presented in Figs. 5 and 9 are with conservative variables and DG0 and the flux presented. In both cases, the pressure contours are smooth and correspond to the incompressible solution [10].

Similar to the results of Guillard and Viozat, the finite volume method (see Figs. 3 and 7) and the discontinuous Galerkin finite element method with the HLLC flux (see Figs. 4 and 8), the pressure contours are not accurate for very low Mach numbers and the solution at Mach number 10^{-1} is the closest to the incompressible solution.

4.2. Internal low speed nozzle (ILSN) at Mach 0.036 and 0.0036

Flows in nozzles are widely studied in the literature. This test case has the advantage of having an analytical solution. We consider a flow in a weakly convergent-divergent nozzle with an infinite upstream Mach number, respectively, of 0.036 or 0.0036, and therefore small compared to 1. By neglecting the viscous effects, it is possible to determine the analytical

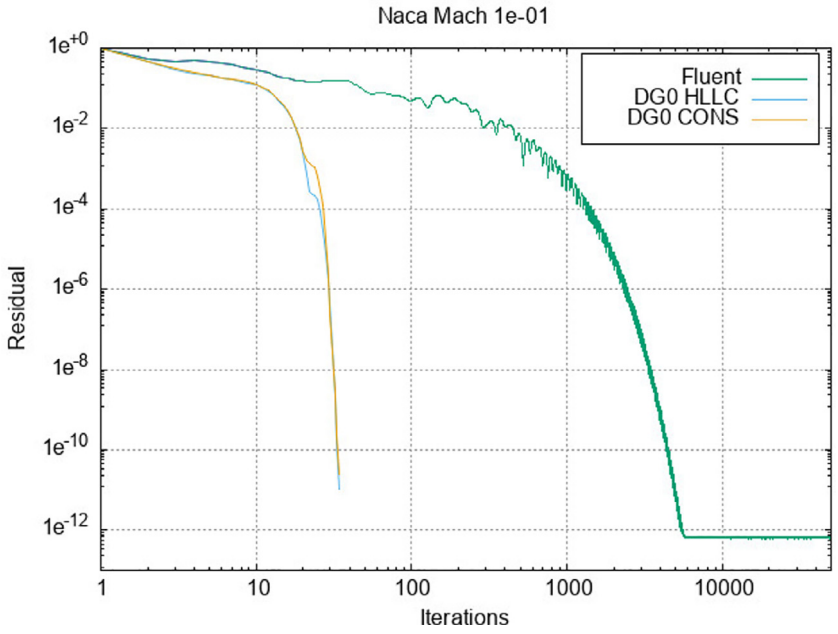

Fig. 6. Normalized residuals for computation of flow around NACA0012 airfoil at Mach 10^{-1}.

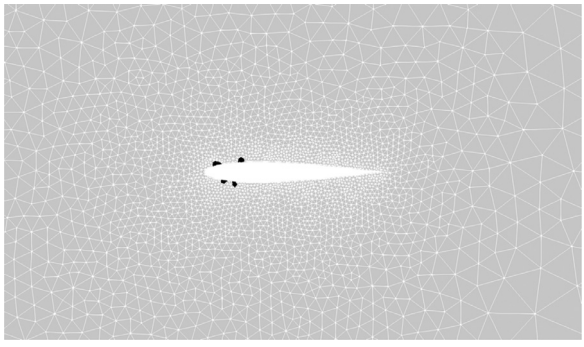

Fig. 7. Pressure field NACA0012 airfoil at Mach 10^{-3}, Fluent, $p_{\min} = 714285$ Pa, $p_{\max} = 714286$ Pa.

solution of this 1D flow despite the 2D character of the nozzle [27]. The expected solution is the steady-state solution of a very subsonic flow under atmospheric conditions. It is therefore reasonable to think that the fluid behaves very similarly to an incompressible fluid.

The nozzle studied here (see Fig. 11) is 1 m long and 0.1 m in diameter at the inlet and outlet. The diameter at the neck is 0.09 m. The mesh used for the computation is a structured mesh composed of 2352 triangular cells, symmetrical with respect to the horizontal axis.

The results obtained for the infinite upstream Mach number 0.036 (see Figs. 12 and 13) are all in good agreement with the analytical solution. At a lower infinite upstream Mach number 0.0036 Figs. 15 and 16), the finite volumes method does not catch the pressure variation but the other solutions correspond to the analytical solution.

The residuals for these simulations are plotted in Figs. 14 and 17. Like for the Naca test case, we try to reach a normalized residual lower than 10^{-12}. With the finite elements methods, convergence is achieved in 20 iterations and the finite volume method needs 100 times more iterations. However, the cost of an iteration is not the same with the finite volumes and finite elements methods. A more complete study should be conducted with the computational time to know the quickest method.

5. Comparison of different sets of variables at low Mach number

In order to evaluate the contribution of the use of primitive and entropy variables compared with conservative variables, the new formulation is benchmarked on previous test cases with higher-order DG discretization (i.e. DG1).

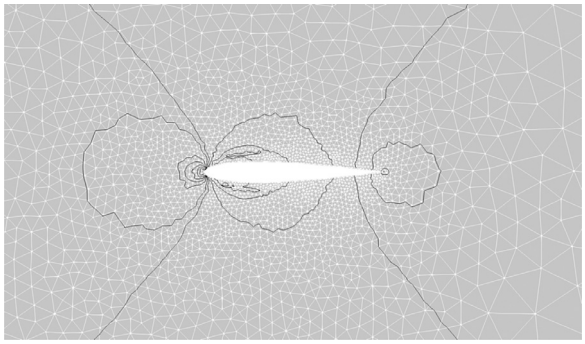

Fig. 8. Pressure field NACA0012 airfoil at Mach 10^{-3}, DG0 HLLC, $p_{\min} = 714285$ Pa, $p_{\max} = 714286$ Pa.

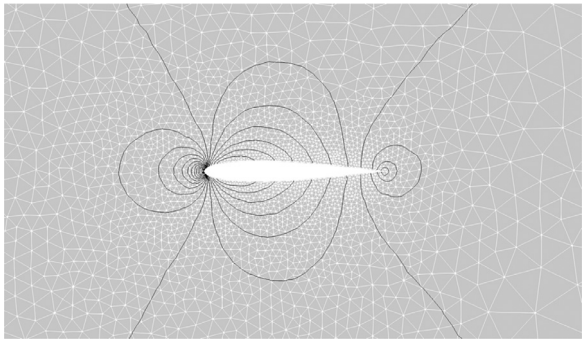

Fig. 9. Pressure field NACA0012 airfoil at Mach 10^{-3}, DG0 CONS, $p_{\min} = 714285$ Pa, $p_{\max} = 714286$ Pa.

Table 4
Summary of test cases.

Test case	Mach number	Compressibility	State	Analytical solution
Naca0012 airflow	10^{-4} to 10^{-1}	Incompressible	Steady	No
Internal low spedd nozzle	0.0036 and 0.036	Incompressible	Steady	Yes

Table 5
Relative L^2 norms of the errors with respect to the analytical solution for ILSN. Simulation of a flow in a nozzle at Mach number 0.036 with DG1 finite elements method and different sets of variables.

	Mach number	Pressure
	(% with respect to conservative variables)	
Conservative	$1.0357293e^{-3}$	$1.85655e^{-2}$
Primitive	$1.0357276e^{-3}$ (− 0.0001%)	$1.85658e^{-2}$ (0.002%)
Entropy	$1.0357214e^{-3}$ (− 0.0007%)	$1.85669e^{-2}$ (0.007%)

The test cases cover a range of low Mach number, from 10^{-4} to 10^{-1}. All these test cases are non-viscous flows, without thermal diffusion and stationary. There is a description in Table 4.

In order to compare the methods and see the differences between them, the simulations are performed on a coarse mesh and without mesh convergence.

5.1. Internal low speed nozzle (ILSN) at Mach 0.036 and 0.0036

The internal low-speed nozzle studied here is the one in Section 4.2. The results obtained for both infinite upstream Mach number 0.036 and 0.0036 are all in good agreement with the analytical solution and superimposed. In each case, we try to reduce the normalized residual to values below 10^{-12}. They are plotted in Figs. 18 and 19.

A relative L^2 norm of the errors with respect to the analytical solution is presented in Tables 5 and 6.

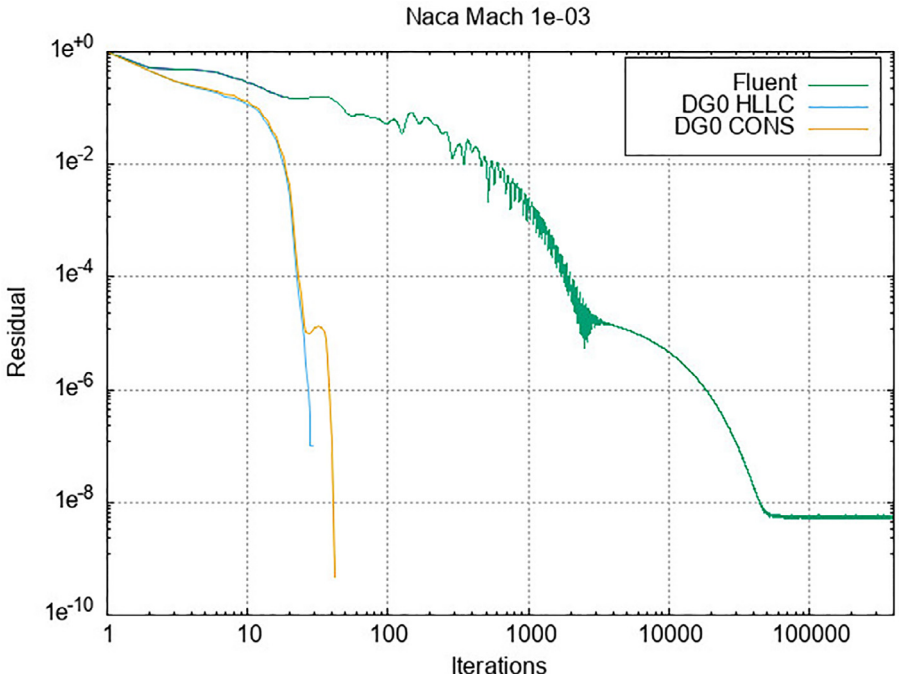

Fig. 10. Normalized residuals for computation of flow around NACA0012 airfoil at Mach 10^{-3}.

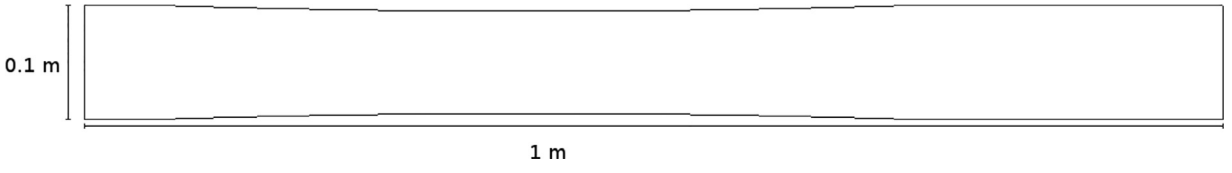

Fig. 11. Computational domain for ILSN nozzle.

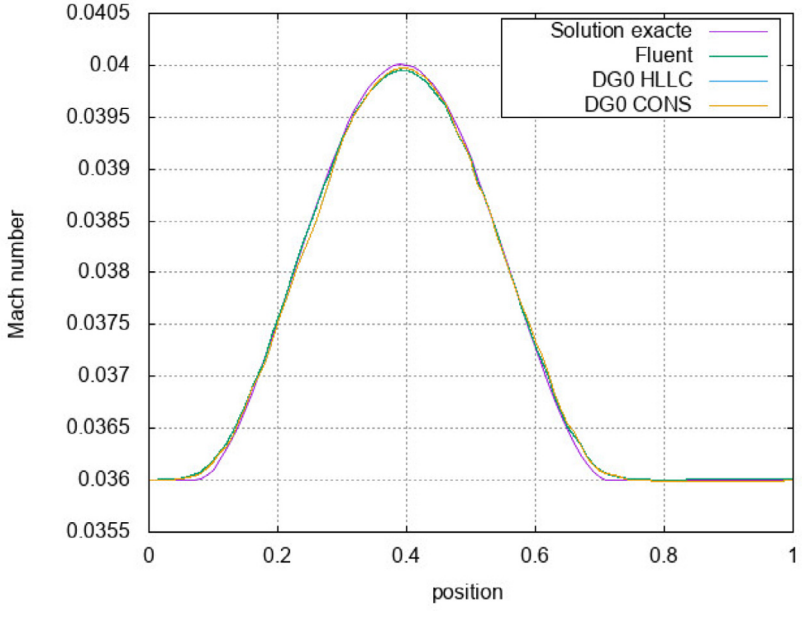

Fig. 12. Evolution of the Mach on the central axis of the nozzle. Inlet Mach number: 0.036.

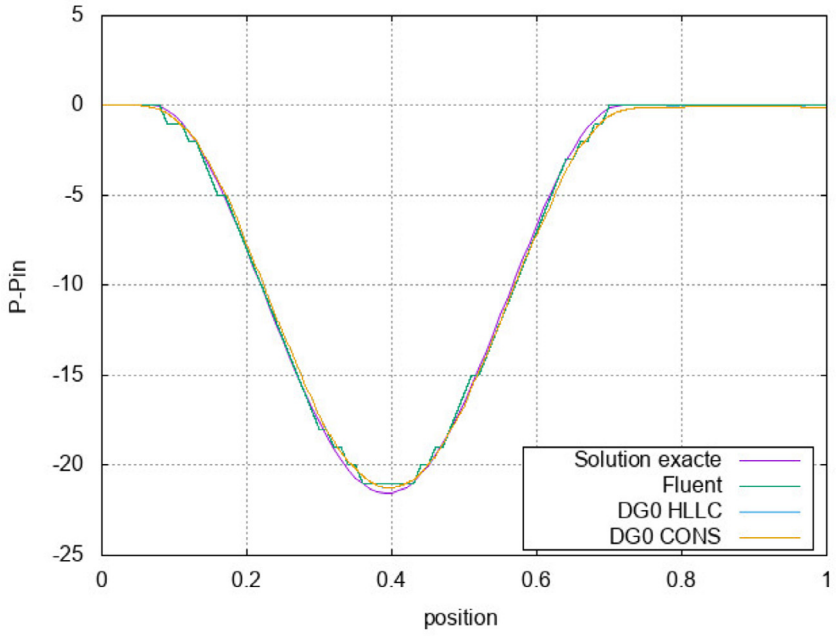

Fig. 13. Evolution of the pressure on the central axis of the nozzle minus the initial pressure (101300 Pa). Inlet Mach number: 0.036.

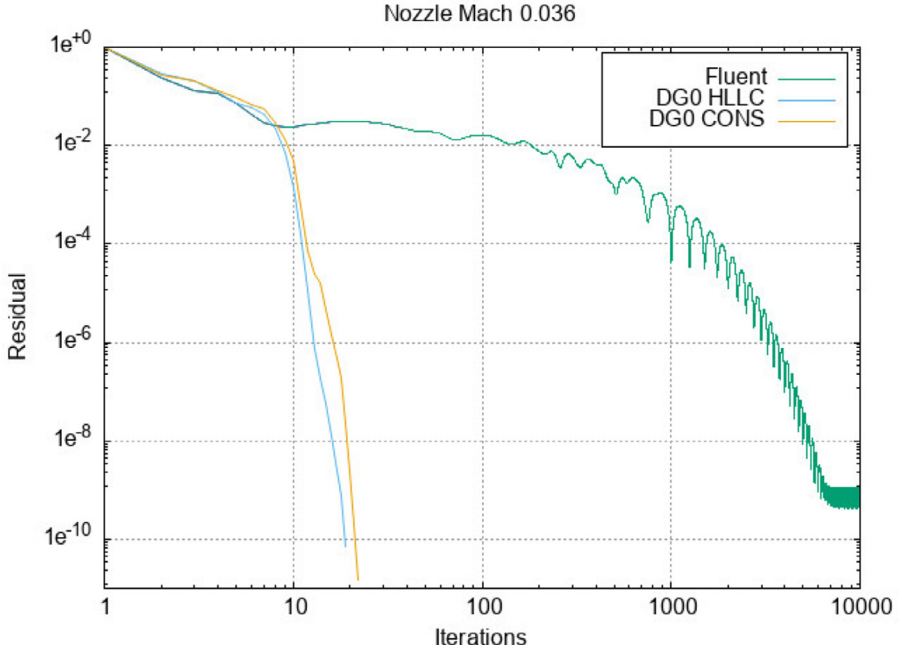

Fig. 14. Normalized residuals for computation of flow in ISLN nozzle at Mach 0.036.

Table 6
Relative L^2 norms of the errors with respect to the analytical solution for ILSN. Simulation of a flow in a nozzle at Mach number 0.036 with DG1 finite elements method and different sets of variables.

	Mach number	Pressure
	(% with respect to conservative variables)	
Conservative	$1.0361418e^{-3}$	$9.90094082908e^{-1}$
Primitive	$1.0361418e^{-3}$ (0%)	$9.90094082908e^{-1}$ (0%)
Entropy	$1.0361436e^{-3}$ (0.0002%)	$9.90094082908e^{-1}$ (0%)

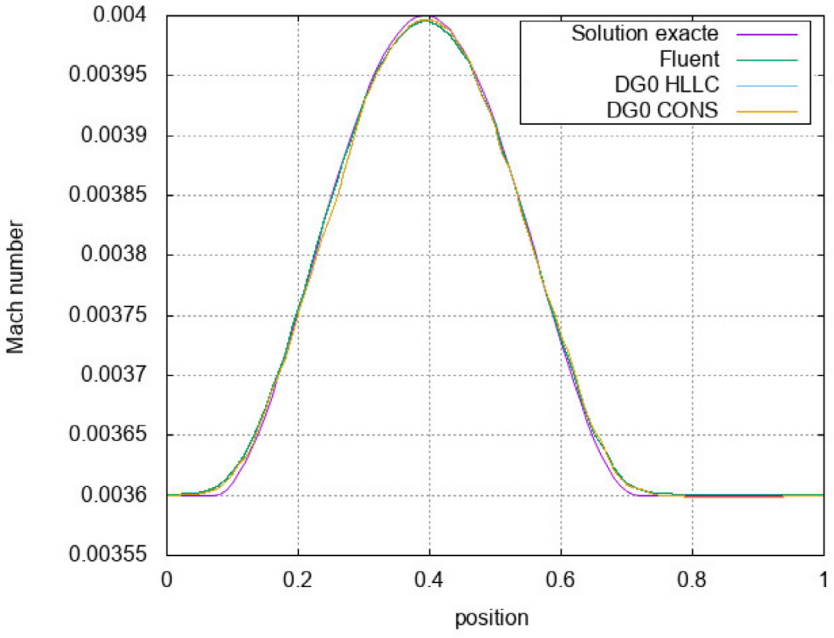

Fig. 15. Evolution of the Mach on the central axis of the nozzle. Inlet Mach number: 0.0036.

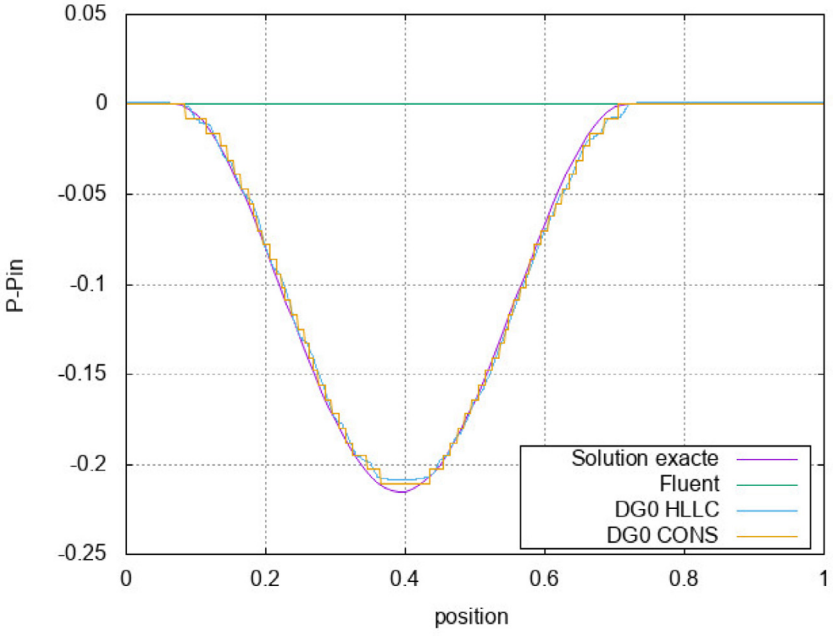

Fig. 16. Evolution of the pressure on the central axis of the nozzle minus the initial pressure (101300 Pa). Inlet Mach number: 0.0036.

5.2. Naca0012 airflow

Like in Section 4.1, we studied a flow around a NACA0012 airflow at several low Mach numbers. The dimensionless inflow velocity and density are set equal to one. The inflow pressure is chosen such that the Mach number is between 10^{-1} and 10^{-4}. Figs. 20–23show the residual of the simulations. In every case we converge as much as possible in order to reduce the normalized residual to values below 10^{-12}. Here, the comparison of the solution is made on the entropy. For this incompressible test case, the entropy must be constant in the whole field. The relative L^2 norms of the errors with respect to the infinite upstream value are shown in Table 7. Whatever the set of variables and whatever the Mach number, results are the same. However, the lower the Mach number the smaller the difference.

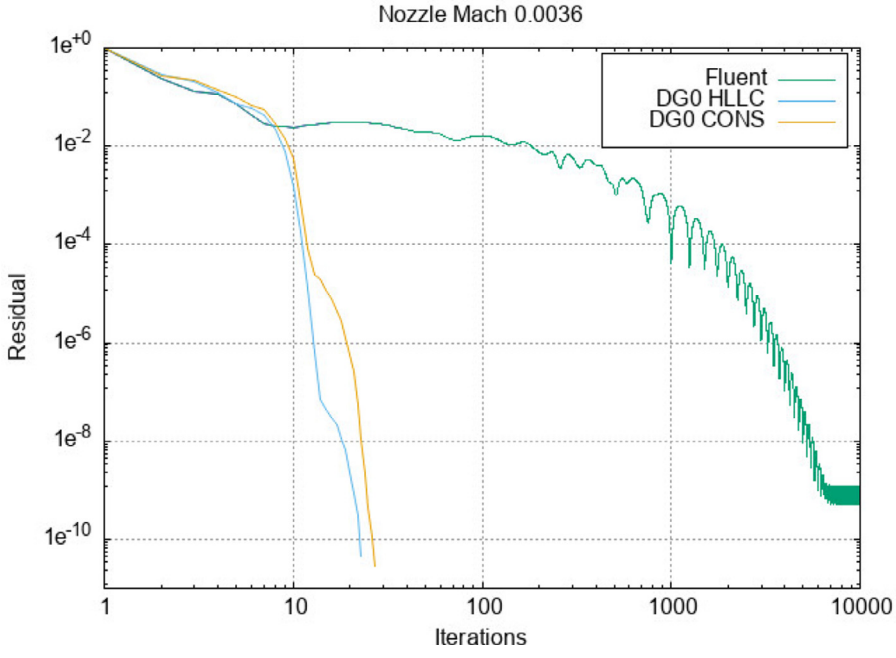

Fig. 17. Normalized residuals for computation of flow in ISLN nozzle at Mach 0.0036.

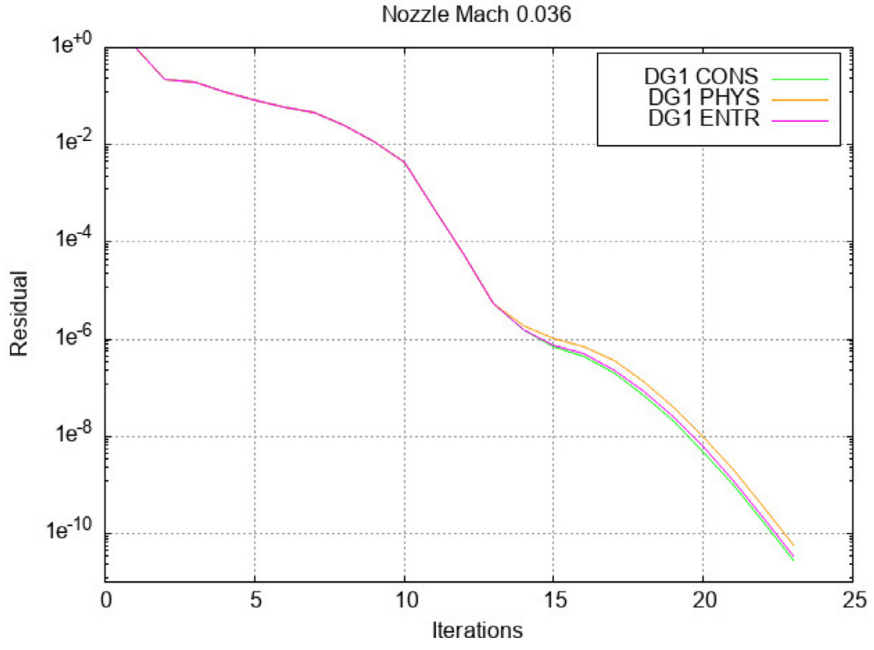

Fig. 18. Normalized residuals for computation of flow in ISLN nozzle at Mach 0.036.

Table 7
Relative L^2 norms of the errors with respect to the infinite upstream value for Naca0012 airflow.

	Entropy ($M = 0.1$)	Entropy ($M = 0.01$)	Entropy ($M = 0.001$)	Entropy ($M = 0.0001$)
	(% with respect to conservative variables)			
Conservative	$7.228e^{-5}$	$7.304e^{-7}$	$3.257e^{-8}$	$4.200e^{-8}$
Primitive	$7.720e^{-5}$ (6.81%)	$7.770e^{-7}$ (6.38%)	$3.256e^{-8}$ (− 0.03%)	$4.200e^{-8}$ (0%)
Entropy	$7.519e^{-5}$ (4.03%)	$7.473e^{-7}$ (2.31%)	$3.257e^{-8}$ (0%)	$4.200e^{-8}$ (0%)

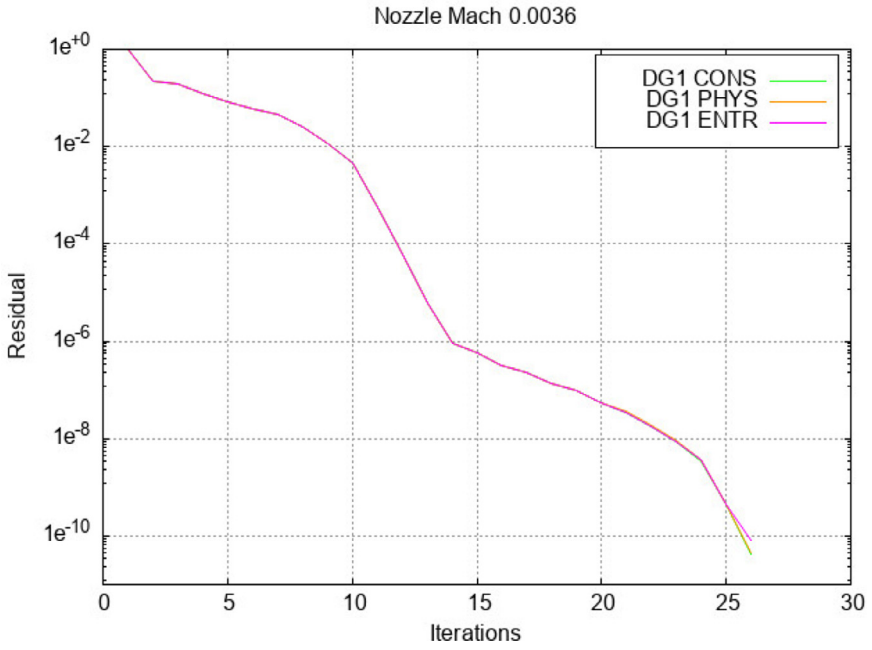

Fig. 19. Normalized residuals for computation of flow in ISLN nozzle at Mach 0.0036.

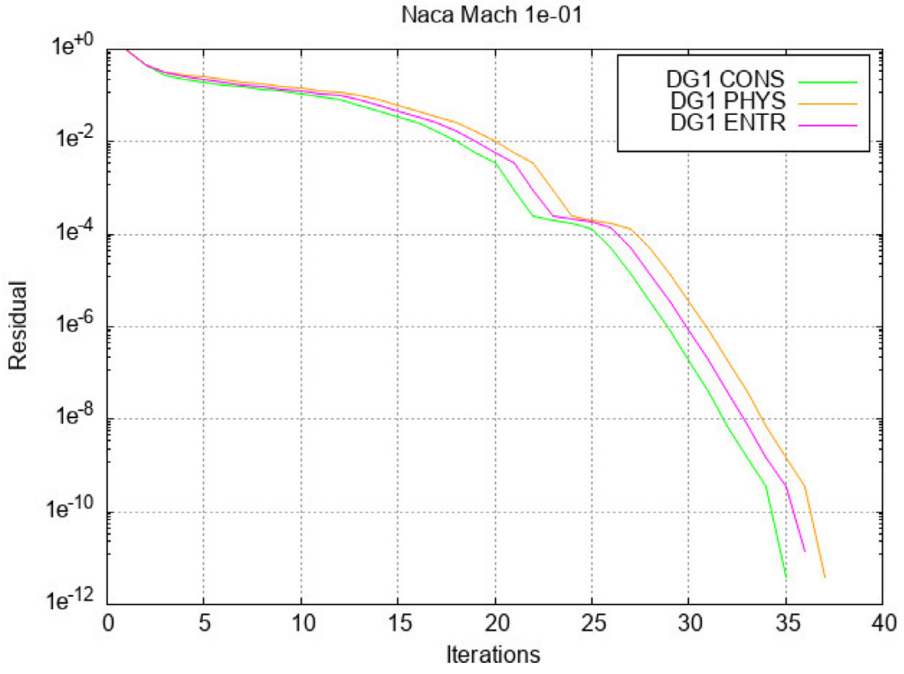

Fig. 20. Normalized residuals for computation of flow around NACA0012 airfoil at Mach 10^{-1}.

6. Conclusion

In this article we have generalized the numerical flux for the discontinuous Galerkin method proposed by Barth to physical and conservative variables in the case of the low Mach number limit. A new numerical flux consistent with all the possible set of variables used in CFD has been performed. Comparisons of different variables are carried out with entropy variables in particular and results are satisfactory. The presented High DG method combined with a dedicated flux shows

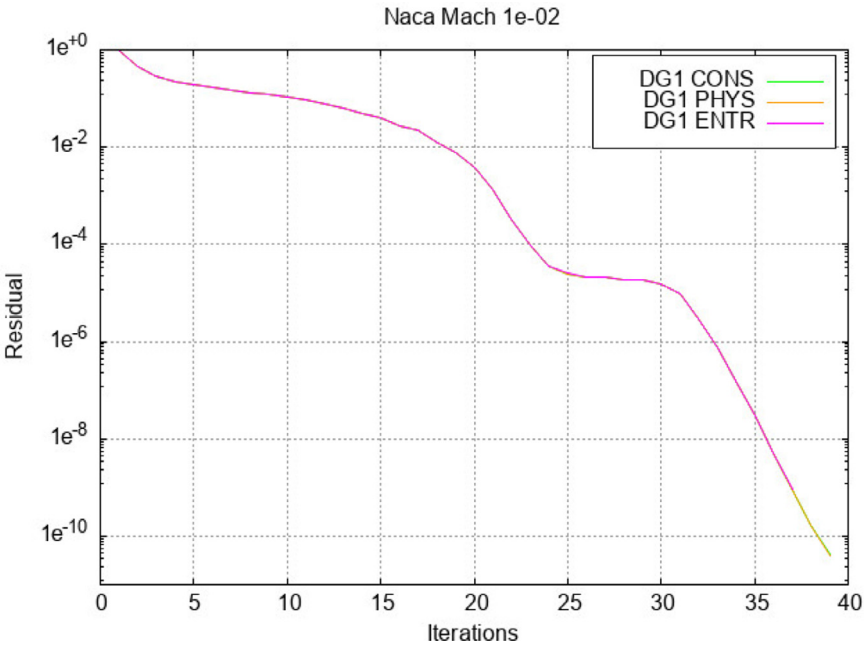

Fig. 21. Normalized residuals for computation of flow around NACA0012 airfoil at Mach 10^{-2}.

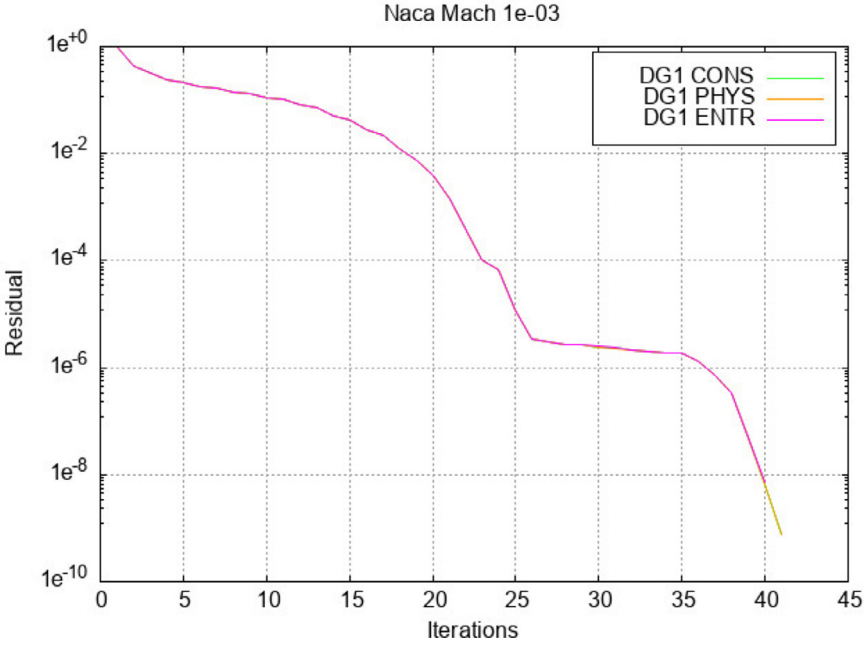

Fig. 22. Normalized residuals for computation of flow around NACA0012 airfoil at Mach 10^{-3}.

accurate results whatever the set of variables. Comparison with the standard numerical HLLC flux in conservative variables shows satisfactory behavior. Furthermore, we have shown that our approach outperforms the standard finite volume methods in FLUENT at very low Mach numbers. Whatever the set of variables with high order DG1 discretization, results are the same at low Mach number for the compressible Euler equations. This leads us to believe that we are on track to reach an all-Mach number solver.

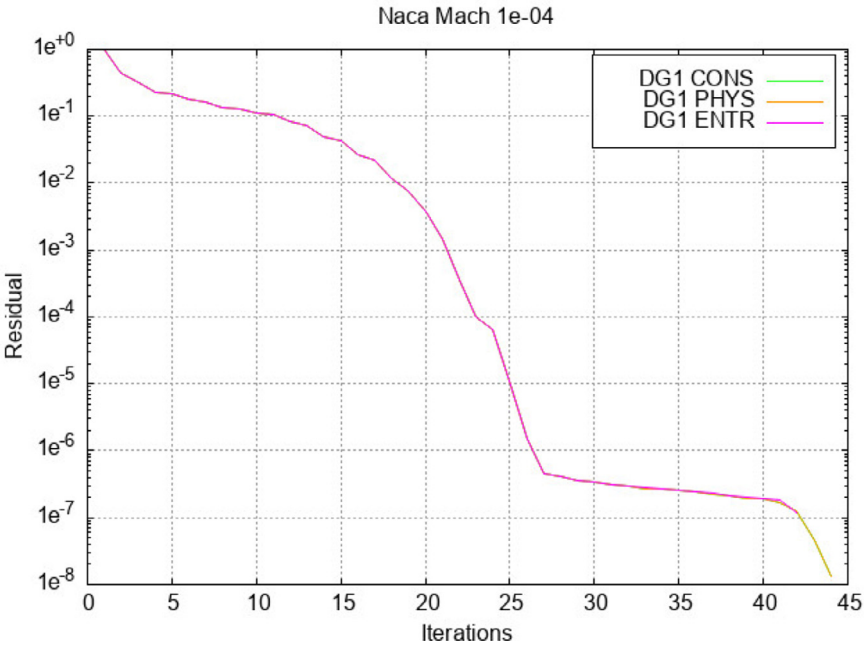

Fig. 23. Normalized residuals for computation of flow around NACA0012 airfoil at Mach 10^{-4}.

Declaration of Competing Interest

The authors declare that they have no known competing financial interests or personal relationships that could have appeared to influence the work reported in this paper.

Acknowledgments

The authors would like to thank professor Jaap van der Vegt from the Department of Applied Mathematics of the University of Twente for his collaboration on this work.

Appendix A

Here we present the Jacobians of the Euler equations expressed in the different sets of variables. The expressions are given for the 2D case with ideal gas law.

The following notations are used for physical quantity : ρ, $V = (V_1, V_2)^{\mathrm{T}}$, T and p for respectively : the density, the velocity, the temperature and the pressure. The total energy is noted $E = e + \frac{1}{2}|V|^2$ with e the internal energy and enthalpy H. c_p, c_V and R are respectively specific heat at constant pressure, specific heat at constant volume and the ideal gas constant.

The Jacobian with conservative variables

The Jacobian of the change of variables:

$$A_0(u) = \frac{\partial u}{\partial u} = \begin{pmatrix} 1 & 0 & 0 & 0 \\ 0 & 1 & 0 & 0 \\ 0 & 0 & 1 & 0 \\ 0 & 0 & 0 & 1 \end{pmatrix} \tag{40}$$

The Jacobian of the Euler flux:

$$A_1(u) = \frac{\partial f_1(u)}{\partial u} = \begin{pmatrix} 0 & 1 & 0 & 0 \\ \frac{1}{2}\frac{R}{c_V}|V|^2 - V_1^2 & \left(2 - \frac{R}{c_V}\right)V_1 & \frac{-R}{c_V}V_2 & \frac{R}{c_V} \\ -V_1V_2 & V_2 & V_1 & 0 \\ V_1\left(\frac{1}{2}\frac{R}{c_V}|V|^2 - H\right) & H - \frac{R}{c_V}V_1^2 & \frac{-R}{c_V}V_1V_2 & \frac{c_p}{c_V}V_1 \end{pmatrix} \tag{41}$$

$$A_2(u) = \frac{\partial f_2(u)}{\partial u} = \begin{pmatrix} 0 & 0 & 1 & 0 \\ -V_1V_2 & V_2 & V_1 & 0 \\ \frac{1}{2}\frac{R}{c_V}|V|^2 - V_2^2 & \frac{-R}{c_V}V_1 & \left(2-\frac{R}{c_V}\right)V_2 & \frac{R}{c_V} \\ V_2\left(\frac{1}{2}\frac{R}{c_V}|V|^2 - H\right) & \frac{-R}{c_V}V_1V_2 & H - \frac{R}{c_V}V_2^2 & \frac{c_p}{c_V}V_2 \end{pmatrix} \tag{42}$$

The Jacobian with primitive variables

The Jacobian of the change of variables:

$$A_0(y) = \frac{\partial u(y)}{\partial y} = \frac{1}{RT}\begin{pmatrix} 1 & 0 & 0 & \frac{-p}{T} \\ V_1 & p & 0 & \frac{-pV_1}{T} \\ V_2 & 0 & p & \frac{-pV_2}{T} \\ E & pV_1 & pV_2 & \frac{-p|V|^2}{2T} \end{pmatrix} \tag{43}$$

The Jacobian of the Euler flux:

$$A_1(y) = \frac{\partial f_1(y)}{\partial y} = \frac{1}{RT}\begin{pmatrix} V_1 & p & 0 & \frac{-pV_1}{T} \\ V_1^2 + RT & 2pV_1 & 0 & \frac{-pV_1^2}{T} \\ V_1V_2 & pV_2 & pV_1 & \frac{-pV_1V_2}{T} \\ V_1H & p(H+V_1^2) & pV_1V_2 & \frac{-pV_1|V|^2}{2T} \end{pmatrix} \tag{44}$$

$$A_2(y) = \frac{\partial f_2(y)}{\partial y} = \frac{1}{RT}\begin{pmatrix} V_2 & 0 & p & \frac{-pV_2}{T} \\ V_1V_2 & pV_2 & pV_1 & \frac{-pV_1V_2}{T} \\ V_2^2 + RT & 0 & 2pV_2 & \frac{-pV_2^2}{T} \\ V_2H & pV_1V_2 & p(H+V_2^2) & \frac{-pV_2|V|^2}{2T} \end{pmatrix} \tag{45}$$

The Jacobian with entropy variables

Calculating the entropy Jacobian is easier after calculating that of the change in variables from primitive ones to entropy. We start with its inverse:

$$\frac{\partial v(y)}{\partial y} = \begin{pmatrix} \frac{R}{p} & \frac{-V_1}{T} & \frac{-V_2}{T} & \frac{-H+|V|^2}{T^2} \\ 0 & \frac{1}{T} & 0 & \frac{-V_1}{T^2} \\ 0 & 0 & \frac{1}{T} & \frac{-V_2}{T^2} \\ 0 & 0 & 0 & \frac{1}{T^2} \end{pmatrix} \tag{46}$$

$$\Rightarrow \frac{\partial y(v)}{\partial v} = \begin{pmatrix} \frac{p}{R} & \frac{pV_1}{R} & \frac{pV_2}{R} & \frac{pH}{R} \\ 0 & T & 0 & V_1T \\ 0 & 0 & T & V_2T \\ 0 & 0 & 0 & T^2 \end{pmatrix} \tag{47}$$

The Jacobian of the change of variables:

$$A_0(v) = \frac{\partial u(v)}{\partial v} = \frac{p}{R^2T}\begin{pmatrix} 1 & V_1 & V_2 & E \\ & V_1^2 + RT & V_1V_2 & V_1H \\ & & V_2^2 + RT & V_2H \\ sym & & & HE + \frac{1}{2}|V|^2RT \end{pmatrix} \tag{48}$$

The Jacobian of the Euler flux:

$$A_1(v) = \frac{\partial f_1(v)}{\partial v} = \frac{p}{R^2T}\begin{pmatrix} V_1 & V_1^2 + RT & V_1V_2 & V_1H \\ & V_1(V_1^2 + 3RT) & V_2(V_1^2 + RT) & V_1^2(RT+H) + RTH \\ & & V_1(V_2^2 + RT) & V_1V_2(RT+H) \\ sym & & & V_1H(RT+H) \end{pmatrix} \tag{49}$$

$$A_2(v) = \frac{\partial f_2(v)}{\partial v} = \frac{p}{R^2T}\begin{pmatrix} V_2 & V_1V_2 & V_2^2+RT & V_2H \\ & V_2(V_1^2+RT) & V_1(V_2^2+RT) & V_1V_2(RT+H) \\ & & V_2(V_2^2+3RT) & V_2^2(RT+H)+RTH \\ sym & & & V_2H(RT+H) \end{pmatrix} \tag{50}$$

Description of symbols and operators

$[\cdot]$	the jump
$\{\cdot\}$	the mean
$v \cdot w = v^{\mathsf{T}} w$	the Euclidian scalar product for $u, v \in \mathbb{R}^n$ (which are column vectors)
$\lvert\cdot\rvert$	the norm of a column vector
A^{T}	the transpose of a matrix $A \in \mathbb{R}^{n\times m}$
Df	the Jacobian matrix of a differentiable function f
$\mathcal{H}$	a family of admissible regular meshes in the usual sense
$\mathcal{K}_h$	cells of a mesh h
$\mathcal{S}_h^{\text{int}}$	the set of interior faces of a mesh h
$\mathcal{S}_h^{\partial}$	the set of boundary faces of a mesh h
$\lvert K\rvert$	the measure of a cell K
$\lvert S\rvert$	the measure of a face S
n_S	a fixed unit vector normal to a face S
f_n^{Σ}	an interior flux
f_n^{∂}	a boundary flux
$\langle\cdot,\cdot\rangle$	scalar product
$u(w)$	the change of variable from w to u

References

[1] Temam R. On the Euler equations of incompressible perfect fluids. J. Funct. Anal 1975;20(1):32–43. doi:10.1016/0022-1236(75)90052-X.
[2] Barth TJ. Numerical methods for gas dynamic systems on unstructured meshes. In: An introduction to recent developments in theory and numerics for conservation laws (Freiburg/Littenweiler, 1997). In: Lect. Notes Comput. Sci. Eng., vol. 5. Berlin: Springer; 1999. p. 195–285.
[3] Bova SW, Carey GF. An entropy variable formulation and applications for the two-dimensional shallow water equations. Int J Numer Methods Fluids 1996;23(1):29–46.
[4] Hauke G, Hughes TJR. A comparative study of different sets of variables for solving compressible and incompressible flows. Comput Methods Appl Mech Eng 1998;153(1):144. http://www.sciencedirect.com/science/article/pii/S0045782597000431.
[5] Pesch L, van der Vegt JJW. A discontinuous Galerkin finite element discretization of the Euler equations for compressible and incompressible fluids. J Comput Phys 2008;227(11):5426–46. doi:10.1016/j.jcp.2008.01.046. http://linkinghub.elsevier.com/retrieve/pii/S0021999108000831.
[6] Winters AR, Gassner GJ. Affordable, entropy conserving and entropy stable flux functions for the ideal MHD equations. J Comput Phys 2016;304:72–108.
[7] Kim SD, Lee BJ, Lee HJ, Jeung I-S. Robust HLLC Riemann solver with weighted average flux scheme for strong shock. J Comput Phys 2009;228(20):7634–42.
[8] Roe PL. Approximate Riemann solvers, parameter vectors, and difference schemes. J Comput Phys 1981;43(2):357–72.
[9] Fluent A. Ansys fluent. Acad Res Release 2015;14:357–72.
[10] Guillard H, Viozat C. On the behaviour of upwind schemes in the low Mach number limit. Comput Fluids 1999;28(1):63–86. doi:10.1016/S0045-7930(98)00017-6. http://www.sciencedirect.com/science/article/pii/S0045793098000176.
[11] Guillard H, Murrone A. On the behavior of upwind schemes in the low mach number limit: II. Godunov type schemes. Comput Fluids 2004;33(4):655–75.
[12] Lions P-L, Masmoudi N. Incompressible limit for a viscous compressible fluid. J Math Pures Appl 1998;77(6):585.
[13] Hoteit H, Ackerer P, Mosé R, Erhel J, Philippe B. New two-dimensional slope limiters for discontinuous Galerkin methods on arbitrary meshes. Int J Numer Methods Eng 2004;61(14):2566–93.
[14] Schochet S. The compressible Euler equations in a bounded domain: existence of solutions and the incompressible limit. Commun Math Phys 1986;104(1):49–75.
[15] Kennel CF, Blandford RD, Coppi P. MHD Intermediate Shock Discontinuities. Part 1. Rankine-Hugoniot Conditions. J Plasma Phys 1989;42(part 2):299–319.
[16] Corrias L. Fast Legendre–Fenchel transform and applications to Hamilton–Jacobi equations and conservation laws. SIAM J Numer Anal 1996;33(4):1534–58.
[17] Mock MS. Systems of conservation laws of mixed type. J Differ Equ 1980;37(1):70–88.
[18] Godunov SK. An interesting class of quasilinear systems. SovMathDokl 1961;2:947–9.
[19] Godunov SK. The problem of a generalized solution in the theory of quasilinear equations and in gas dynamics. Russian Math Surv 1962;17(3):145.
[20] Fletcher CAJ. A primitive variable finite element formulation for inviscid, compressible flow. J Comput Phys 1979;33(3):301–12.
[21] Tadmor E. Entropy stability theory for difference approximations of nonlinear conservation laws and related time-dependent problems. Acta Numer 2003;12:451–512. doi:10.1017/S0962492902000156. http://www.journals.cambridge.org/abstract_S0962492902000156.
[22] Massey BS. Units, dimensionnal analysis and physical. Van Nostrand Reinhold Company; 1971. ISBN 0442051786
[23] Kok J. An industrially applicable solver for compressible, turbulent flows. Delph University of Technology; 1998. Ph.D. thesis.
[24] Barth TJ. Numerical methods for gasdynamic systems on unstructured meshes. In: An introduction to recent developments in theory and numerics for conservation laws. Springer; 1999. p. 195–285. http://link.springer.com/chapter/10.1007/978-3-642-58535-7_5.
[25] Barth TJ. Simplified discontinuous Galerkin methods for systems of conservation laws with convex extension. In: Discontinuous Galerkin methods. Springer; 2000. p. 63–75. http://link.springer.com/chapter/10.1007/978-3-642-59721-3_3.
[26] Schall E, Chauchat N. Implicit method and slope limiter in AHMR procedure for high order discontinuous Galerkin methods for compressible flows. Commun Nonlinear Sci Numer Simul 2019;72:371–91.
[27] Candel S. Mcanique des fluides. Dunod; 1995. ISBN 2-10-002585-6.